Heat Transfer and Flow Transitions of Thermal Plumes Generated by Double Heating Elements in a Confined Enclosure

*WANG Ying**, *XU Zhejian*, *YANG Wen*, *MA Xinyu*

Sino-European Institute of Aviation Engineering, Civil Aviation University of China, Tianjin 300300, P. R. China

(Received 16 September 2025; revised 15 November 2025; accepted 19 December 2025)

Abstract: The buoyancy-induced flow constitutes a core scientific issue for thermal management of electronic devices and thermal design of energy systems, where accurate characterization of flow and heat transfer is essential to improve thermal efficiency. In this work, buoyancy-induced flow above two heating elements flush-mounted at the bottom of a square enclosure containing air is numerically investigated over a range of Rayleigh numbers ($0 < Ra \leqslant 1.5 \times 10^8$), with a focus on equal and unequal heat flux conditions under a constraint of constant total thermal energy input. Distinct flow transitions are observed in both cases, leading to the identification of three flow regimes: Steady, periodic unsteady, and chaotic unsteady. Two types of periodic flows are distinguished, in which the first is a periodic flow dominated by a fundamental frequency (FF) and its integer-multiple frequencies (INTMF), while the second is a more complex periodic flow featuring FF, INTMF, and their sub-harmonics. The transitions between these regimes are affected by the relative heat flux of the two heaters. When the heat flux of the two heaters is unequal, the range of Rayleigh numbers corresponding to periodic flow is suppressed. It is also found that the time-averaged maximum temperature of the strong heater increases more rapidly with Ra, while that of the weak heater increases more slowly, reflecting the interaction between buoyancy-driven flow dynamics and asymmetric heat input. Analysis of the time-averaged Nusselt number demonstrates that heat dissipation from the isothermal walls remains roughly equivalent, even when the heat flux of the two heaters differs by a factor of two. These findings highlight the critical roles of Rayleigh number, the number of heaters, and the heat flux ratio of the heaters in determining heat transfer and flow characteristics for buoyancy-driven convection systems, providing important theoretical support and design references for engineering scenarios such as electronic devices and design of new energy systems.

Key words: natural convection; thermal plume; double heating elements; flow transitions; heat transfer

CLC number: V211.3 **Document code**: A **Article ID**: 1005-1120(2026)01-0095-15

0 Introduction

Thermal plumes generated by heat sources within a confined enclosure are phenomena which can be found in many industrial and engineering fields. For instance, overheating in electronic devices[1], movement of hot toxic gases during fire combustion[2-3], energy storage in materials[4], nuclear reactor designs[5], etc. Over the past few decades, extensive reviews have reported the confined thermal plume from a single heat source. Due to the confinement, it is found that the bifurcated states are readily set up due to the sensibility to thermal forcing and boundary conditions. Desrayaud and Lauriat[6] previously investigated buoyancy-induced plumes above a horizontal line heat source inside a rectangular vessel. They identified a sequence of flow transitions such as Hopf and pitchfork bifurcations as well as transitions to quasi-periodic and chaotic regimes. Concurrently, Fiscaletti et al.[7] carried out an experiment within a water-filled cavity containing a horizontal cylindrical heat source. The sys-

*Corresponding author, E-mail address: wang_y@cauc.edu.cn.

How to cite this article: WANG Ying, XU Zhejian, YANG Wen, et al. Heat transfer and flow transitions of thermal plumes generated by double heating elements in a confined enclosure[J]. Transactions of Nanjing University of Aeronautics and Astronautics, 2026, 43(1): 95-109.

http://dx.doi.org/10.16356/j.1005-1120.2026.01.008

tem is witnessed to undergo a transition from steady-state, laminar flow to unsteady oscillatory flow, which can be referred as natural swaying motion. Later, Hernández[8] investigated numerically confined thermal plumes from a single heat source, and found that the oscillatory solutions exhibited particular eigen modes (frequency and wavelength) which depended on the fluid physical properties, the amplitude of the forcing parameter and box dimensions. In recent studies, Barrios et al.[9] analyzed flow transitions of a confined thermal plume by using Fourier power spectrum of a suitable quantity, called asymmetry. The results show an identification of the fundamental frequency and the appearance of harmonics and other frequencies. Wang et al.[10] investigated an unsteady confined thermal plume initiated by a linear heat source. The transition to unsteadiness through a supercritical Hopf bifurcation was determined in their study. Additionally, turbulent plumes were also addressed in literature. Bastiaans et al.[11] studied a 3D turbulent plume in a confined environment by both DNS and LES. The results indicate that buoyancy force has a strong impact on the turbulence production and evolution process. George et al.[12] presented a numerical study of a turbulent line plume in a confined region. They observed that the plume dynamical centreline was deviating from its geometrical centreline. This centreline deviation is due to the swaying motion of the plume and its meandering along the heat source direction. Later on, the same authors[13] studied the wall-attached plume in a confined region, and proposed a modified version of the Baines and Turner model developed by Baines and Turner[14] to account for wall shear stress. Chai et al.[15] simulated turbulent natural convection in a rectangular enclosure with a curved surface heated from below. A correlation was proposed to predict the averaged Nusselt number as a function of the Rayleigh number (Ra).

The above-mentioned works not only account for the behaviors of thermal plumes under different flow regimes, but also focus on exploring the flow transitions of thermal plumes (i.e., the dynamic evolution from laminar flow to oscillatory flow, and further to turbulent flow). While these studies have yielded abundant findings, they are limited to single-heat-source configurations and thus not applicable to engineering scenarios involving multiple heat sources, such as the passive cooling of electronic devices using natural convection[16-17]. In an early work, Gebhart et al.[18] studied experimentally the interactive process between unequal laminar plumes generated by line heat sources. They found that these flows were affected by other similar flows which interfered with the supply of entrainment fluid. Ichimiya and Saiki[19] analyzed the behavior of two steady thermal plumes from two heated portions on the bottom of an enclosure and found that the flow patterns of thermal plumes were related to the pitch of two heated portions. Banerjee et al.[20] carried out steady simulations on natural convection in a bi-heater configuration. The influences of heater length and heater strength ratios on heat transfer were discussed in details. Later, Biswas et al.[21] investigated buoyancy-driven flow occurring in the presence of protruded heater by varying heater aspect ratio, Pr and Ra. It was seen that, the flow structures in the case of air were symmetric within $Ra \leqslant 10^6$ for both the single and double heaters. In addition, with the increase in heater height although the total flow decreases, a consistent trend of increasing heat transfer is observed. Several studies[22-26] have been conducted on the interactive process of turbulent plumes above multiple heat sources. Cenedese and Linden[22] proposed a model to predict the total volume flux and entrainment of the two coalescing turbulent plumes and compared the simulated and experimental results. Gao et al.[25] and Yang et al.[26] investigated the interaction of thermal plumes generated by two equal heat sources, and both of their works analyzed the touching height of the two plumes at different spacings of heat sources. Yin et al.[27-28] carried out a challenging study considering triple equal starting thermal plumes from volumetric heat sources, with particular emphasis on the effects of heat source strength and spacing. They adopted 2D particle image velocimetry (PIV) to monitor the full evolution process of thermal plumes from their initial formation to upward penetration, classifying the entire developmental process into four distinct

regimes: Relatively isolated development, bending wall flows, development after a self-merged state, and evolution with global merging. They further revealed that the spacing of the multi-heat-source system dictated the timing of plume coalescence, whereas heat source strength governed the ascending height of the merged plumes. However, the existing research on multi-plumes has neither rigorously explored the flow transition dynamics triggered by heat flux variations nor quantitatively evaluated the potential impacts of asymmetric heat source distribution on flow stability.

Thus, the main objective of the present study is to investigate the flow transitions in multi-plume systems and the corresponding variations in heat transfer. As a fundamental case for exploring multi-plume behaviors, we focus on unsteady thermal plumes generated by two heaters, with particular attention paid to scenarios involving unequal heat flux conditions of the heaters. The paper is organized as follows: The physical problem and the governing equations are briefly presented in Section 1. The numerical methods and associated validations are introduced in Section 2. The main results regarding flow transitions with varying Ra and heat flux ratio are discussed in Section 3. Conclusions are provided in Section 4.

1 Physical Problem and Governing Equations

1.1 Problem description

The computational model simulates two heat sources releasing thermal energy into a two-dimensional square cavity. Fig.1 illustrates the geometry and thermal boundary conditions.

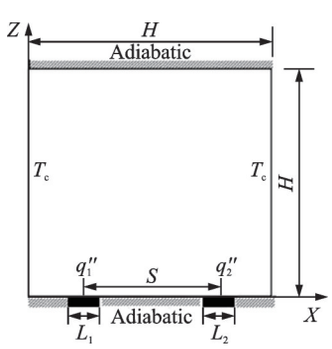

Fig.1 Schematic of the physical system

The top wall and non-heated portions of the bottom wall are adiabatic, and the two vertical sidewalls maintain a constant temperature T_c. The working fluid is air ($Pr=0.71$). The side length of the cavity is H and there are two finite-sized heaters at the bottom with the length of $L_1=L_2=0.2H$. The generated heat fluxes are q_1'' and q_2'', respectively, defining the heat flux ratio $q_r=q_2''/q_1''$. The distance between the centerlines of the two heaters is $S=0.5H$. All walls are treated as rigid no-slip boundaries. The characteristic temperature difference is defined as $\Delta T=Q'/\lambda$, with λ denoting the thermal conductivity of the air, and $Q'=q_2''L_1+q_2''L_2$ representing the input total heat flux. It is also noteworthy that the relatively low temperature difference (no more than 1.5 K) encountered in the present work makes the Boussinesq approximation entirely legitimate.

1.2 Governing equations

The governing equations for mass, momentum and energy are

$$\frac{\partial u_i}{\partial x_i}=0 \tag{1}$$

$$\frac{\partial u_i}{\partial t}+\frac{\partial(u_iu_j)}{\partial x_j}=-\frac{\partial p^*}{\partial x_i}+Pr\frac{\partial^2 u_i}{\partial x_j^2}+RaPr\theta\delta_{iz} \tag{2}$$

$$\frac{\partial \theta}{\partial t}+\frac{\partial(\theta u_j)}{\partial x_j}=\frac{\partial^2\theta}{\partial x_j^2} \tag{3}$$

where $x_i=(x, z)$ denotes the coordinate components normalized with respect to the characteristic domain size H; $u_i=(u, w)$ represents the dimensionless velocity components in the x- and z- directions, which are non-dimensionalized by the diffusive velocity α/H, with α being the thermal diffusivity; θ is the dimensionless temperature, defined as $\theta=(T-T_c)/\Delta T$; and p^* is the dimensionless effective pressure, scaled as

$$p^*=\frac{p+\rho_{ref}gzH}{\rho_{ref}(\alpha/H)^2} \tag{4}$$

where p is the static pressure and ρ_{ref} the density at the reference state.

In the governing equations, two dimensionless quantities Pr and Ra appear. The first is the Prandtl number defined as

$$Pr=\nu/\alpha \tag{5}$$

where ν is the kinematic viscosity. The second dimensionless parameter is the Rayleigh number given by

$$Ra = \frac{g\beta\Delta TH^3}{\nu\alpha} \tag{6}$$

with β the coefficient of thermal expansion measured at the reference temperature $T_{ref} = T_c$.

The convective Nusselt numbers of the left and right isothermal walls of the cavity are defined as

$$Nu_l = \int_0^1 \left(\frac{\partial\theta}{\partial x}\right)_{x=0} \mathrm{d}z \tag{7}$$

$$Nu_r = -\int_0^1 \left(\frac{\partial\theta}{\partial x}\right)_{x=1} \mathrm{d}z \tag{8}$$

Energy conservation requires that the net heat input from the bottom heaters equals the net heat transfer rate through the vertical walls, yielding the following relationship between the Nusselt numbers on the opposing vertical walls.

$$\langle Nu_{total}\rangle = \langle Nu_l\rangle + \langle Nu_r\rangle = 1 \tag{9}$$

where $\langle\cdot\rangle$ indicates time-averaged values for unsteady regimes.

2 Numerical Modeling

2.1 Numerical methods

The open-source software Code Saturne is used to solve the governing equations via the finite volume method. For spatial discretization, the second-order linear upwind (SOLU) scheme discretizes velocity in the momentum equations, while temperature in the energy equation uses a second-order central difference scheme. Time integration employs the first-order backward Euler method. For momentum-pressure coupling, we use the semi-implicit method for pressure-linked equations consistent (SIMPLEC), a predictor-corrector method. In order to select an appropriate grid for the physical model shown in Fig.1, three different grid resolutions are tested under $Ra = 1.5 \times 10^8$. The grid distribution is refined in the near wall regions by using a geometric progression. Table 1 compares the time-averaged Nusselt number of the left wall, the maximum values of time-averaged horizontal velocity and time-averaged vertical velocity for the three grids. The results indicate that, when compared with the 61×41 grid, the calculation result obtained from the 121×81 grid is closer to that of the 241×161 grid, with a relative error between them of approximately 1% or less. A time step $\delta t \approx 10^{-5}$ was used in all calculations representing 0.001% of the smallest diffusive time scale $\tau_d = H^2/\alpha$. Therefore, this time step size can be regarded as a small fraction of the characteristic time scale of the thermal phenomenon, while also enabling the resolution of the shortest time scales associated with any developing instabilities.

Table 1 Comparison results on different grids at $Ra = 1.5\times10^8$

Grid size	Time-average Nu_l		Time-average horizontal velocity		Time-average vertical velocity	
	$\langle Nu_l\rangle$	Relative difference/%	$\langle u\rangle_{max}$	Relative difference/%	$\langle w\rangle_{max}$	Relative difference/%
61×41	0.506 0	1.67	687.578 1	6.25	876.935 2	5.82
121×81	0.502 9	0.65	731.057 8	0.32	921.627 3	1.02
241×161	0.499 7		733.426 4		931.086 3	

2.2 Code validation

The code is first validated against the case of steady natural convection in two-dimensional flow and validated in comparison with the results of Banerjee et al[20]. Their work reported steady state simulation of natural convection in a square cavity with two discrete heat sources on the bottom wall, and studied the buoyancy-driven flow by varying length and strength ratios of the two heat sources. Based on the assumption of equal heat source lengths, we simulate the cases of $q_r = 1$ and $q_r = 2$ from their work. The reference utilizes a non-uniform grid of 70×70 cells, whereas we employ a grid of 120×80 cells, densified near the wall. The calculation is carried out at $Ra = 2.9 \times 10^5$. Fig.2 presents the steady-state isotherms of different heat flux ratios. It can be seen that our results are in a good agreement with the literature. For $q_r = 1$, the heat fluxes of the heat-

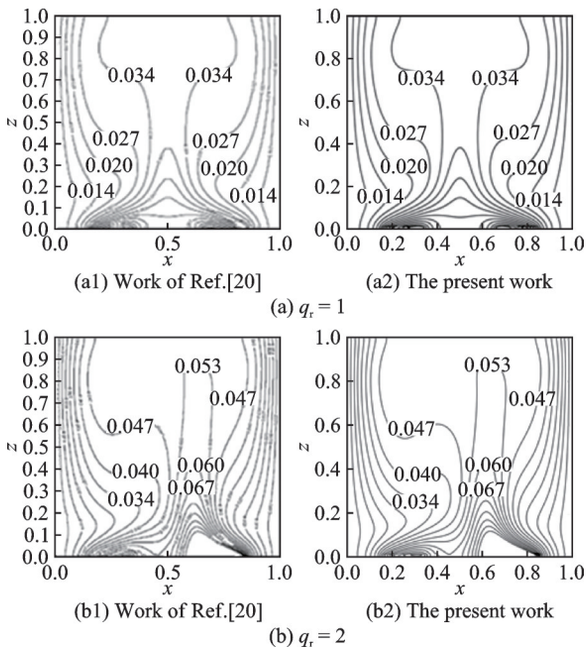

Fig.2 Iso-contours of temperature θ for the cases at $Ra = 2.9 \times 10^5$

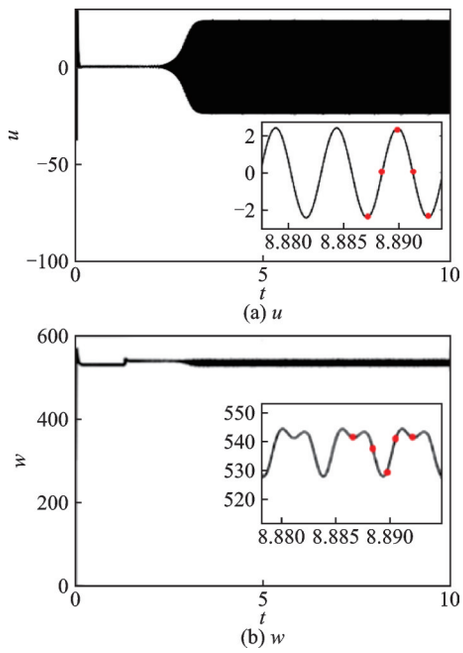

Fig.3 Time evolution of horizontal velocity (u) and vertical velocity (w) at the monitoring point $(x,z)=(0.5,0.5)$ at $Ra = 3 \times 10^7$, starting from $Ra = 2.9 \times 10^5$

ers are equal which induces a symmetrical distribution of isotherms in the cavity. For $q_r = 2$, the heat flux generated by the right heater is twice that of the left heater, which implies that the portion of heat input through the right heater is about 67% of the total heat input. In this case, the symmetrical distribution is broken and the isotherms are closely packed near the right wall, indicating a high heat dissipation.

3 Results and Discussion

3.1 Flow transitions under equal heat flux condition

As a representative case of the flow we are interested in, the Rayleigh number is increased to a specific value $Ra = 3 \times 10^7$ for the case $q_r = 1$ (i.e., heat fluxes of the two heaters are equal), resulting in an unsteady flow. Fig.3 depicts the temporal evolution of the horizontal velocity (u) and vertical velocity (w) at the monitoring point $(x,z)=(0.5,0.5)$, starting from $Ra = 2.9 \times 10^5$, where the red dots identify the five specific instants displayed in Fig.4. After an initial transient phase resembling a steady state, both velocity components exhibit periodic oscillations with a consistent time-period $t_p \approx 0.005\,4$.

Fig.4 illustrates a cycle of oscillation by the snapshots of the temperature field (top row) and the kinetic energy field (bottom row). These snapshots are taken at the time instants marked by dots in the inset of Fig.3. We observe that the flow field in the near-source region remains relatively stable, whereas the plume heads exhibit periodic swaying behavior along the vertical centerline. This flow stage corresponds to the "evolution with global merging" proposed by Yin et al.[27-28], i.e., the thermal buoyancy-driven flows induced by the two heaters have come together, and the flow field evolves into a fully developed state. It is also observed that the temperature fluctuations as well as velocity fluctuations share the same oscillation frequency. The periodic nature of the swaying motion is further analyzed by means of the normalized power spectra in Fig.5. The spectra (P_w) are given for the velocity component w at three monitoring points. It can be seen that a same fundamental frequency is present with its integer multiples in the both spectra. The fundamental frequency occurs at $f_0 = 184.8$, which corresponds exactly to the reciprocal of the swaying motion period.

In the following, this work considers flow transitions across a range of Rayleigh numbers $0 < Ra \leqslant 1.5 \times 10^8$ for the case $q_r = 1$. The transitions

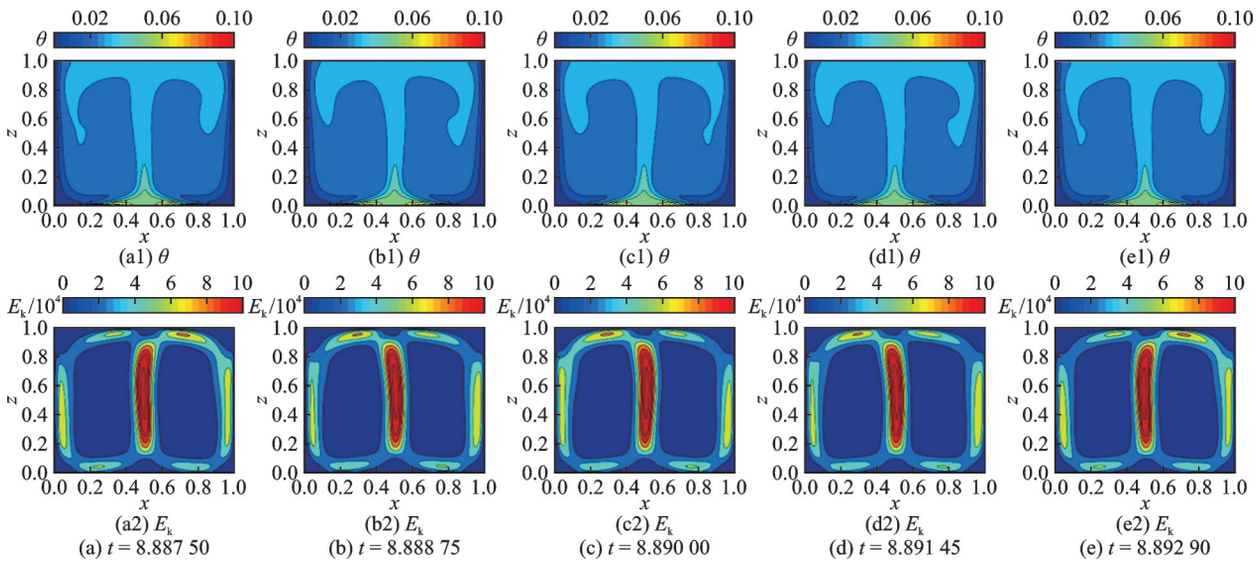

Fig.4 Instantaneous temperature field and kinetic energy field at $Ra = 3 \times 10^7$ for five different instants (Contour interval: 0.005 for isotherms, 20 000 for kinetic energy isovalues)

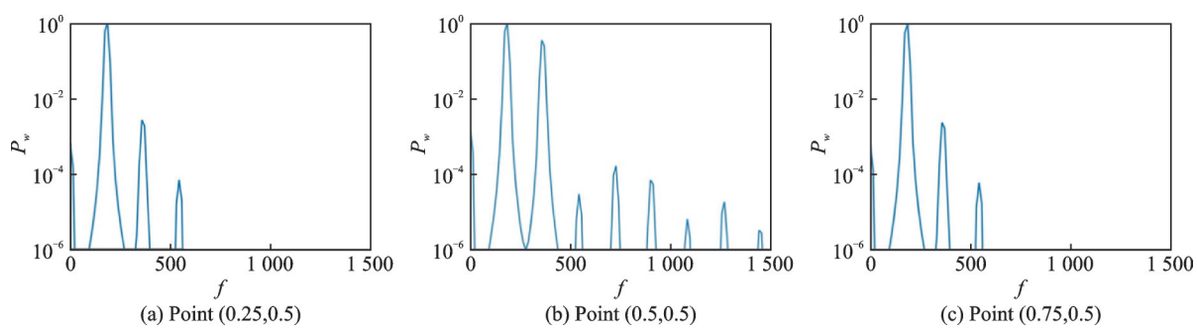

Fig.5 Normalized power spectral density of the vertical velocity (w) at three different points for the periodic flow at $Ra = 3 \times 10^7$

are to be analyzed by giving the features of phase-space trajectories (w-u) and Fourier frequency spectrum. According to the calculation results of this paper, the flow over this Ra range can be divided into three flow patterns, respectively. Table 2 summarizes these results: Steady flow, noted as S; periodical flow with fundamental frequency (FF) and its integer multiples of frequencies (INTMF), noted as MP; more complex periodical flow with FF, INTMF and its sub-harmonics, noted as SMP. A multitude of sub-harmonic waves are excited, and the energy is mainly concentrated in these waves.

Table 2 Behavior about the transition of the thermal plume in the enclosure for the case $q_r = 1$

Interval	Regime
$0 < Ra \leqslant 2.9 \times 10^7$	Steady flow, noted as S
$3 \times 10^7 \leqslant Ra \leqslant 1.3 \times 10^8$	Periodical flow with integer multiples of fundamental frequency, noted as MP
$1.4 \times 10^8 \leqslant Ra \leqslant 1.5 \times 10^8$	Periodical flow with sub-harmonic and integer multiples of FF, noted as SMP

These flow transitions are further illustrated in Fig.6, which presents the power spectra of the w-velocity and phase-space trajectories (w-u) at the center point $(x, z) = (0.5, 0.5)$, yielding deeper insight into the flow dynamics. As shown in Fig.6(a), the flow field in periodical stage only contains FF and INTMF wave motion. As Ra increases, the amplitude of harmonics becomes stronger while the FF increases, in the sequence of 184.8, 204.2, 275.8. Fig.7(a) shows the frequency characteristics in SMP stage. For $Ra = 1.4 \times 10^8$ and $Ra = 1.5 \times 10^8$, the periodic motion is still present, but the sub-harmonic appears that changes the oscillation qualitatively. Such low frequency wave is interaction with FF and INTMF waves. As a result, the flow field is consisted of a family of FF, INTMF and its sub-harmonic frequency multiple. Fig.6(b) and Fig.7(b) present the phase-space trajectories from $Ra = 3 \times 10^7$ to $Ra = 1.5 \times 10^8$. It can be seen that the curves in phase-space are always confined to a two-torus limit-

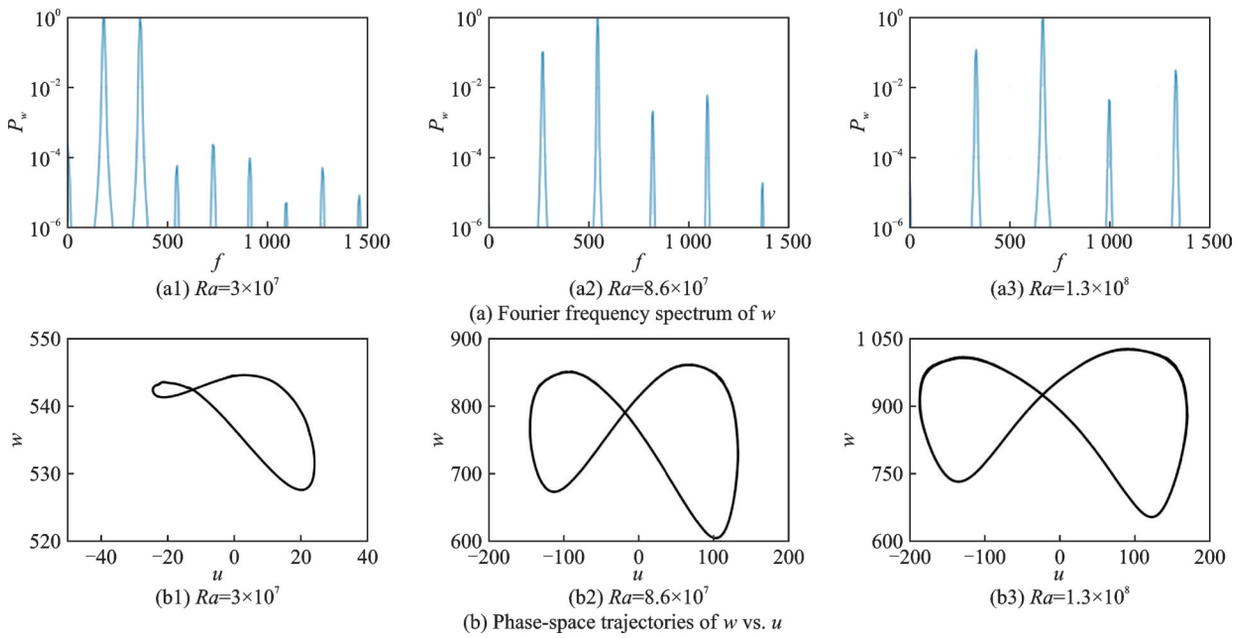

Fig.6 Analysis of flow transitions via Fourier frequency spectrum of w and phase-space trajectories of w vs u for $Ra=3\times10^7$, 8.6×10^7, and 1.3×10^8

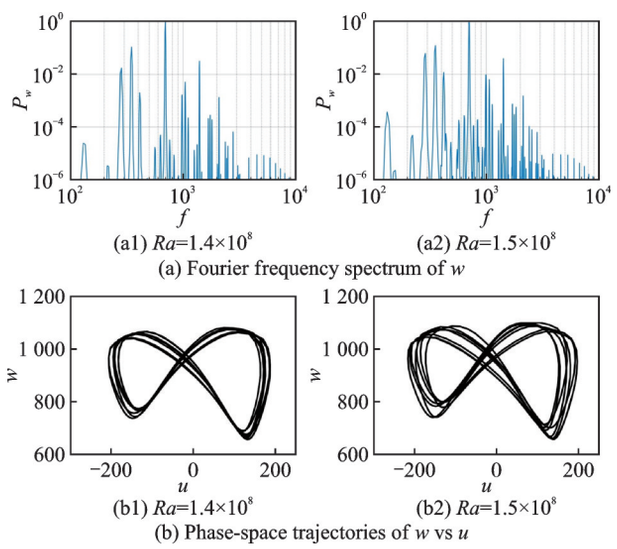

Fig.7 Analysis of flow transitions via Fourier frequency spectrum of w and Phase-space trajectories of w vs u for $Ra=1.4\times10^8$ and 1.5×10^8

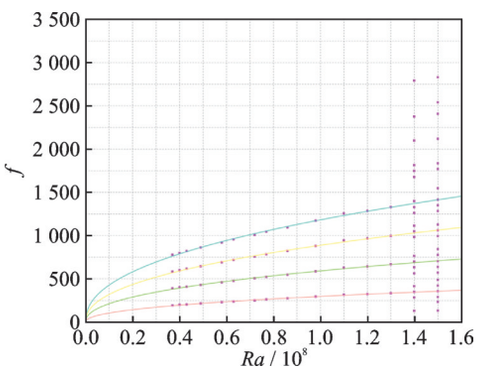

Fig.8 Variation trend of frequencies in the spectrum analysis with Ra number

ed-cycle in the MP stage, and then appear to be thickened in the SMP stage. Although the flow during the SMP stage exhibits complex family waves, it remains a periodical solution owing to the closed curves in phase space.

In Fig.8, we show the frequencies of the power spectra of w that have a power between 10^{-5} and 10^0 as a function of Ra. The fundamental frequency follows the scaling law $f_0=C\cdot Ra^r$, with best-fit parameters, $C=0.072\,11$ and $r=0.451\,86$. The first, second and third harmonic frequencies (represented by continuous lines in red, green, yellow, blue, respectively) exhibit the same $C\cdot Ra^r$ scaling, with their frequencies being interger multiples of the fundamental frequency. At lower Ra values ($Ra<3\times10^7$), the absence of dominant frequencies indicates a steady state regime. As Ra increases to 3×10^7, it appears discontinuous frequencies that increase by multiples of the fundamental frequency, which corresponds to a periodic regime. Within the range of $3\times10^7\leqslant Ra\leqslant1.3\times10^8$, the fundamental frequency rises with Ra by the scaling f_0. In this interval, harmonics are always present and scale with the same tendency of fundamental frequency, which are shown by continuous curves. At higher Ra values ($1.4\times10^8\leqslant Ra\leqslant1.5\times10^8$), the scaling relations are nearly the same as in the previous

interval, but sub-harmonics appear. The instantaneous temperature and kinetic energy distributions at three different time instances for $Ra = 1.5 \times 10^8$ are shown in Fig. 9. It can be observed that the plume structures exhibit significant bending and folding in the temperature field, while the kinetic energy field consistently forms a large-scale recirculation zone. As a result of the developing instabilities, the entire plume undergoes more intense oscillations compared with those in the MP regime (see Fig.4).

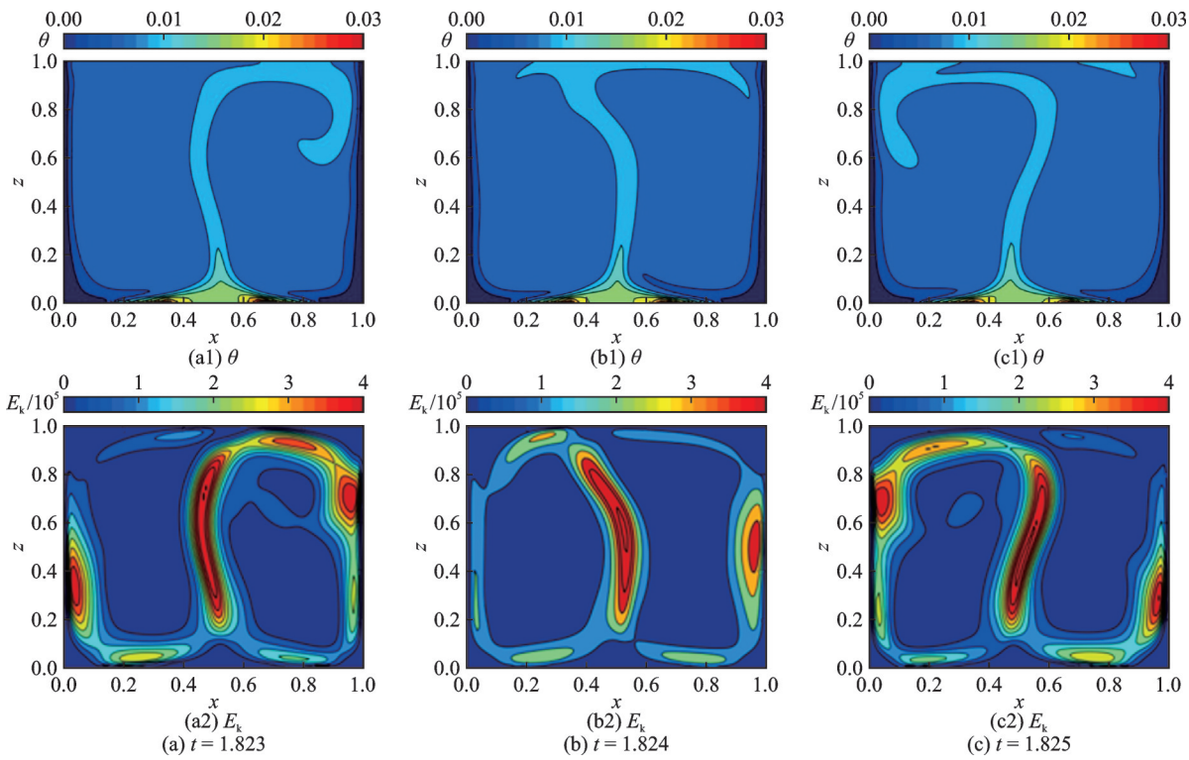

Fig.9 Instantaneous temperature field and kinetic energy field at $Ra = 1.5 \times 10^8$ for different instants (Contour interval: 0.003 for isotherms, 80 000 for kinetic energy isovalues)

3.2 Flow transitions under unequal heat flux condition

Given the relevance to engineering applications involving heaters with non-uniform heat generation, this study proceeds to investigate the configuration with a heater flux ratio of $q_r = 2$. Simulations are initially performed at $Ra = 3 \times 10^7$, where the flow reaches a laminar steady state, as depicted in Fig.10. Notably, however, for this Rayleigh number, results reveal a periodic state under the condition of equal flux strength $q_r = 1$. Additionally, it is observed that the flow transition from steady state to periodic state occurs between $Ra = 5.8 \times 10^7$ and 6.3×10^7 for $q_r = 2$. This finding suggests that the heat flux ratio of the heaters exerts a significant influence on the stability of natural convection. Specifically, when the two heaters operate at unequal heat fluxes, the system exhibits a tendency to transition from unsteady to steady flow.

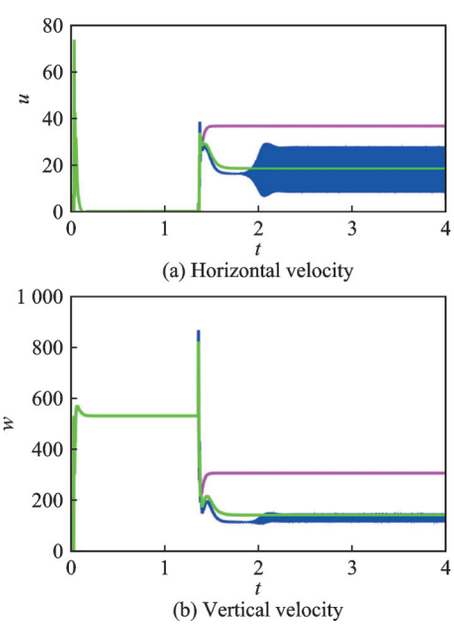

Fig.10 Time evolution of the horizontal velocity (u) and vertical velocity (w) at the monitoring point $(x, z)=(0.5, 0.5)$ for different Rayleigh numbers ($Ra = 3 \times 10^7$ in magenta, $Ra = 5.8 \times 10^7$ in green, $Ra = 6.3 \times 10^7$ in blue)

To further examine the flow characteristics of plumes under the unequal heat flux condition, Figs.11 and 12 present the power spectra of w-velocity and the phase-space trajectories at the center point $(x, z)=(0.5, 0.5)$ over the range of $6.3\times10^7\leqslant Ra\leqslant1.5\times10^8$ (Fig. 11 (a) and Fig. 12 (a). Fig.13 further presents the variation of the dominant frequencies from these power spectra as a function of Ra. The fundamental frequency follows the scaling law $f_0=C\cdot Ra^r$, with best-fit parameters, $C=0.166\,35$ and $r=0.434\,01$. The first, second and third harmonic frequencies (represented by continuous lines in black) exhibit the same $C\cdot Ra^r$ scaling, with frequencies being integer multiples of the fundamental frequency. The presence of the fundamental frequency and its harmonics are clearly observed from $Ra=6.3\times10^7$ to $Ra=7.8\times10^7$, denoting a MP regime. Throughout this range, both the funda-

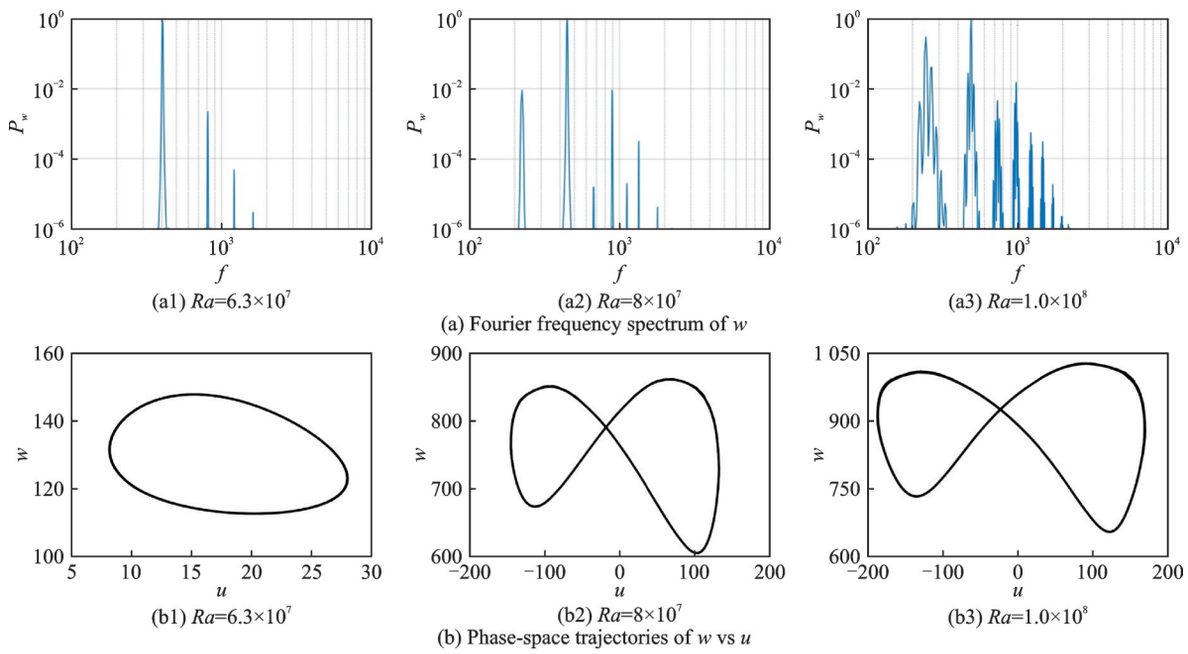

Fig.11 Analysis of flow transitions via Fourier frequency spectrum of w and phase-space trajectories of w vs u for $Ra=6.3\times10^7$, 8×10^7, and 1.0×10^8

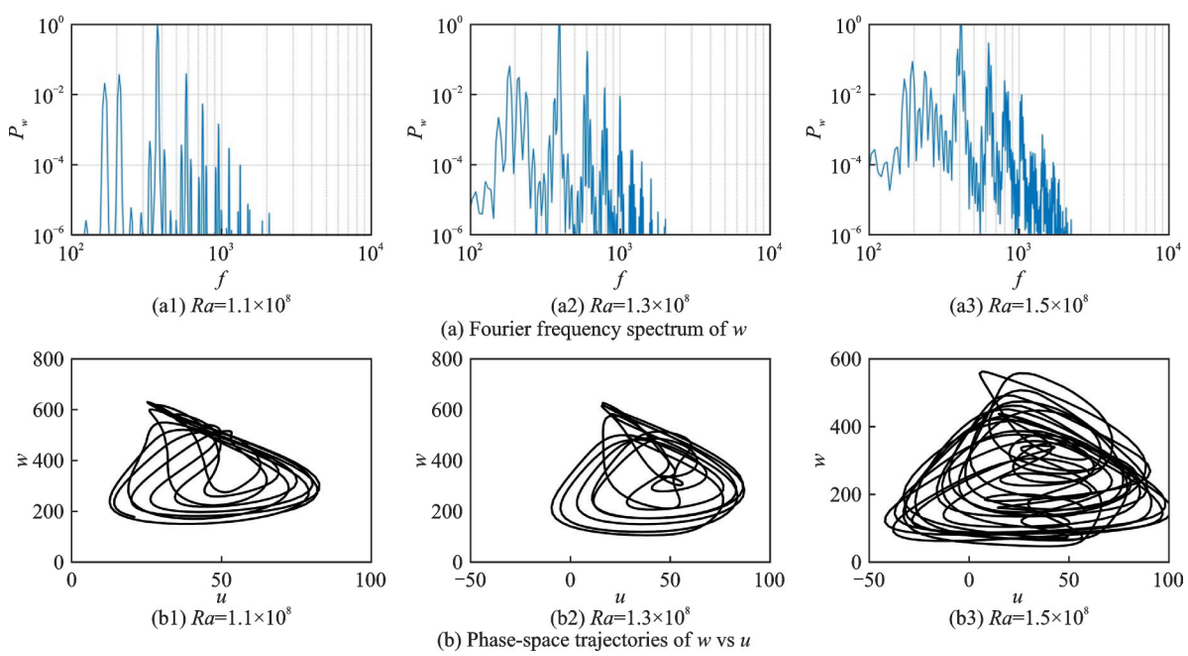

Fig.12 Analysis of flow transitions via Fourier frequency spectrum of w and phase-space trajectories of w vs u for $Ra=1.1\times10^8$, 1.3×10^8, and 1.5×10^8

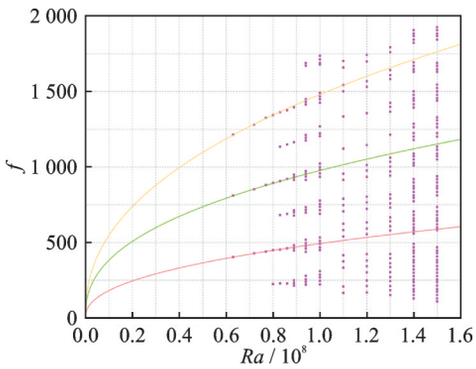

Fig.13 Variation trend of frequencies in the spectrum analysis with Ra number

mental frequency and the harmonics increase with Ra, following a scaling relation of f_0. Subsequently, the sub-harmonics emerges at $Ra = 8.0 \times 10^7$, signifying the system's transition into the SMP stage. For $8.0 \times 10^7 \leqslant Ra \leqslant 1.0 \times 10^8$, the scaling relations are the same as in the previous interval. At $Ra = 1.1 \times 10^8$, the frequencies deviate from this scaling, indicating a breakdown of periodicity. At $Ra = 1.5 \times 10^8$, the spectrum exhibits broadband noise although relatively sharp spectral peaks still exist.

The corresponding phase-space trajectories are shown in Fig.11(b) and Fig.12(b), which initially form overlapping limited-cycles and then gradually separate and thicken. At $Ra = 1.1 \times 10^8$, the phase trajectories are confined within a bounded region but show excursions to other regions. As the Ra number increases further, the complexity of phase-space excursion gradually escalates. The largest Lyapunov exponent (LLE) is subsequently computed for various Ra, utilizing the time-series data of vertical velocity w during the stable oscillating period at the monitoring point. The calculation results show that in all cases, the LLE first exhibits a transient spike followed by rapid convergence. For Ra ranges from 6.3×10^7 to 8×10^7, the LLE eventually converges to 0. At $Ra = 1.1 \times 10^8$, the LLE attains a steady state at a small positive value approaching 0. At $Ra = 1.5 \times 10^8$, the LLE stabilizes within the small positive interval of 0.04—0.05 (see Fig.14, where $t - t_0$ denotes the time elapsed from the initial transient, used for calculating the LLE). Accordingly, it can be determined that for Ra in the range of 1.1×10^8 to 1.5×10^8, the flow regime is non-periodic, more precisely. This range corresponds to the critical transition regime where the flow field evolves from quasi-periodic behavior to a weakly chaotic state.

Fig.15 depicts the distributions of temperature and kinetic energy fields at three different instants for $Ra = 1.5 \times 10^8$. It's observed that asymmetric heating results in heat concentration near the strong heater, with thermal convection being more intense near the strong heater while being weaker near the weak heater. Compared with the case of $q_r = 1$, we find that the overall temperature within the cavity is

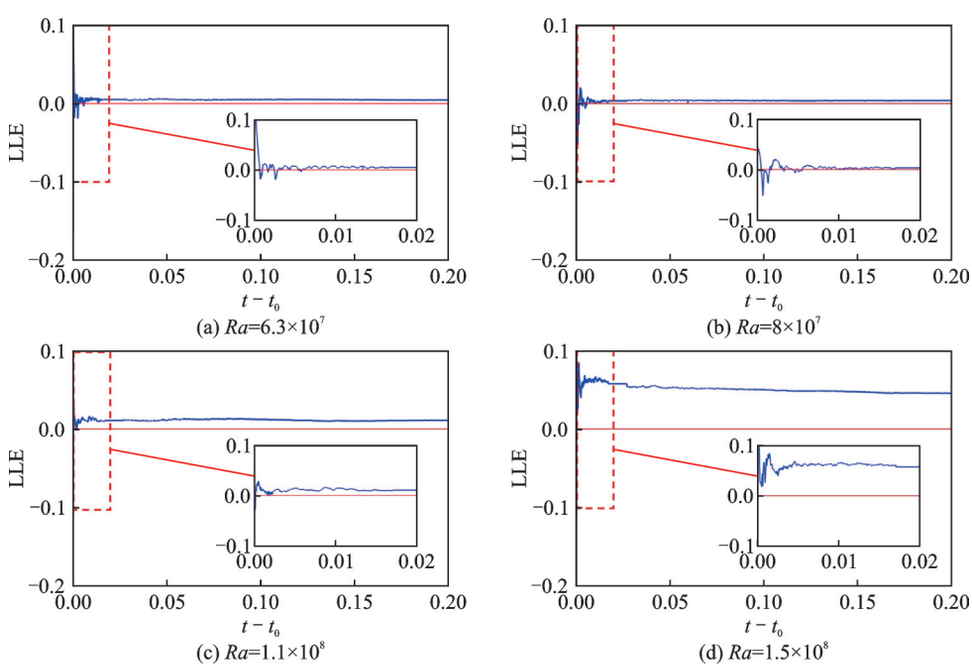

Fig.14 LLE computed from the time-series data of vertical velocity w for $Ra = 6.3 \times 10^7$, 8×10^7, 1.1×10^8, and 1.5×10^8

enhanced. Fig.16 illustrates the division of different flow regime stages with respect to the parameters (Ra, q_r). Due to the constraint that total thermal energy pumps into the cavity remaining unchanged, the flow pattern for the cases with $q_r = 1$ and $q_r = 0.5$ are mirror-symmetric about the enclosure centerline, since the heaters are of the same length. Therefore, the results for $q_r = 0.5$ have also been included in the diagram to enhance the completeness of the results. It is clearly demonstrated that asymmetric heating delays the transition from steady laminar flow to periodic flow. The reason is that periodic flow relies on regular, repeating fluid motion patterns. These patterns are highly susceptible to instability if one heater is much stronger than the other. Consequently, under the unequal heat flux condition, the range of Rayleigh numbers within which periodic flow can be sustained is narrowed. It can thus be inferred that when the heat flux ratio is sufficiently large or small, the periodic stage becomes notably short, ultimately approximating the behavior of a single heater positioned on one side.

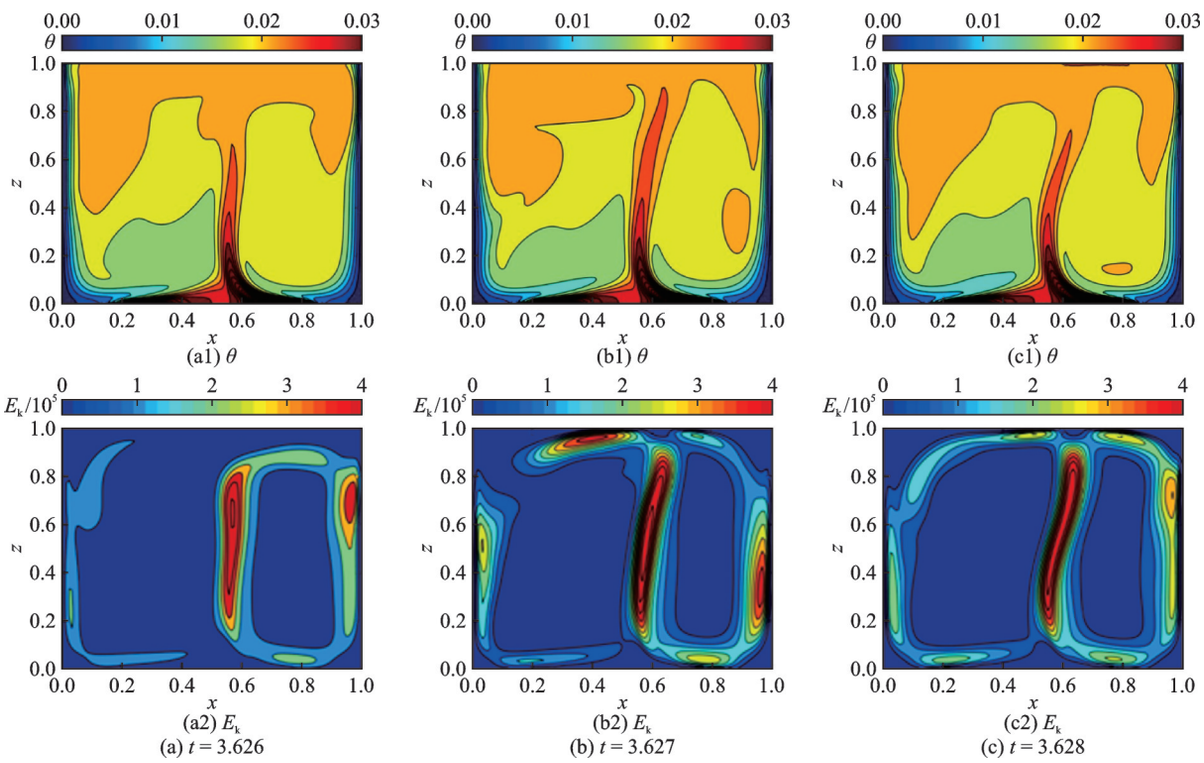

Fig.15 Instantaneous temperature field and kinetic energy field at $Ra = 1.5 \times 10^8$ for different instants (Contour interval: 0.003 for isotherms, 80 000 for kinetic energy isovalues)

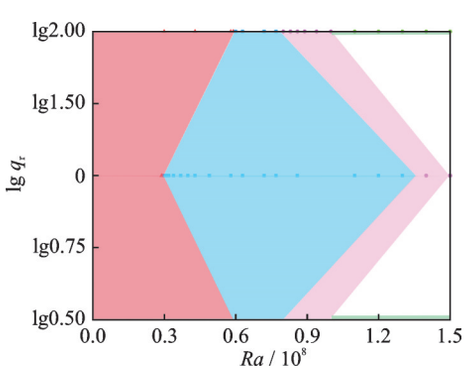

Fig.16 Division of different flow regime stages with respect to the parameters (Ra, q_r) (The red area corresponds to the steady state, blue to the MP stage, pink to the SMP stage, and green to the non-periodic flow)

3.3 Heat transfer

The allowable thermal operation window for reliable performance is a prime constraint for thermal analysis in many engineering applications. Within the permissible temperature range, a priori information on the maximum temperature is vital from a design perspective. Therefore, the variation in the non-dimensional measure of time-averaged maximum temperature with the Rayleigh number, for the cases of $q_r = 1$ and $q_r = 2$ is given in Fig.17. Both quantities follow the scaling relations $\langle Ra \cdot \theta_{max} \rangle = C \cdot Ra^{\gamma}$, and the values of C and γ are shown in

Table 3. Note that taking the product of the Rayleigh number and the non-dimensional maximum heater surface temperature, we obtain $Ra\cdot\theta_{max}=(T_{max}-T_0)g\beta H^3/\nu\alpha$, so that the quantity $Ra\cdot\theta_{max}$ is considered as an appropriate dimensionless measure of the maximum non-dimensional temperature on the surface of a heater. It is observed that the time-averaged values of $Ra\cdot\theta_{max}$ increase with Ra, exhibiting a power law $C\cdot Ra^{\gamma}$. Compared with the case of $q_r=1$, the asymmetric heating leads to a faster increase in the maximum temperature at the strong heater (right heater), whereas the maximum temperature at the weak heater (left heater) increases slower. Essentially, the temperature of the strong heater is more sensitive to Ra, as its heat output surpasses the system's capacity to dissipate heat with increasing convection. In contrast, the weaker heater's lower heat output is more readily managed by the enhanced fluid flow, thereby leading to a diminished temperature response. Furthermore, it is observed that for a given Ra, the heater temperature in the case of $q_r=1$ is approximately the average of the two asymmetric heater temperatures in the case of $q_r=2$.

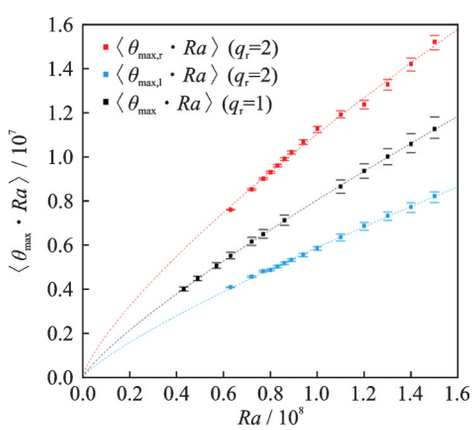

Fig.17 Variation of time-averaged $\langle\theta_{max}\cdot Ra\rangle$ of the left and right heaters together with its standard deviation as a function of Rayleigh number

Table 3 C and γ values of the scaling relation $\langle\theta_{max}\cdot Ra\rangle=C\cdot Ra^{\gamma}$ taken from data of Fig.16

Parameter	$q_r=1$	$q_r=2$	
		Left	Right
C	2.078 86	1.746 84	8.860 12
γ	0.823 50	0.815 99	0.761 98

Fig.18 depicts the time-averaged Nusselt numbers of left wall, right wall, and their sum across different Ra numbers. It can be seen that the values of $\langle Nu_{total}\rangle$ for the two cases remain consistently close to unity, indicating the energy conservation of the system. In the case of $q_r=1$, the Nusselt number on both wall surfaces remains 0.5 due to the symmetric heat input. In contrast, for $q_r=2$, the time-averaged Nusselt number on the left wall is observed to be approximately 0.46, while that on the right wall is around 0.54. This is because the heat transfer at the isothermal walls depends more on the system's total heat budget and the ability of convection.

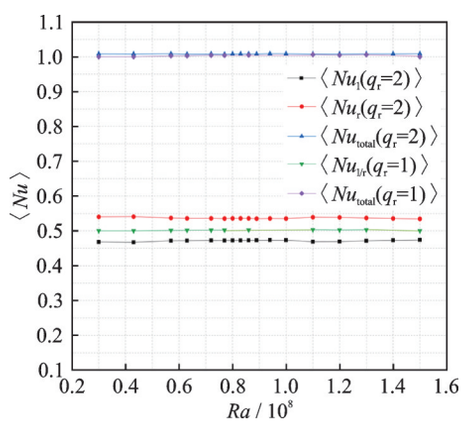

Fig.18 Variation of time-averaged Nusselt numbers of left wall, right wall, and their sum vs Rayleigh number

4 Conclusions

This study examines the flow and heat transfer characteristics of buoyancy-driven convection above two flush-mounted heating elements at the bottom of a two-dimensional square cavity. Simulations have been conducted over a wide range of Rayleigh numbers, $0<Ra\leqslant 1.5\times 10^8$, for both equal and unequal heat flux conditions. Flow transitions are observed in both cases, with three distinct regimes identified: Steady, periodic unsteady, and chaotic unsteady. Two types of periodic flows are distinguished: One is a periodic flow characterized by a fundamental frequency (FF) and its integer-multiple frequencies (INTMF), and the other is a more complex periodic flow involving FF, INTMF, and

sub-harmonic frequency multiples. By analyzing the Fourier power spectrum, the FF and the emergence of harmonics and other frequencies are detected. This study further proposes a relationship between *Ra* and the relevant frequencies in the power spectra. The results reveal that the flow regime is strongly influenced by the heat flux ratio. Under the unequal heat flux condition, the range of *Ra* in which the periodic flow can occur is suppressed. We also show the variations in the time-averaged maximum temperature and Nusselt number as *Ra* increases. While the temperature of the heaters is strongly affected by their relative heat flux, the heat transfer at the isothermal walls depends more on the system's total heat budget and the ability of convection. Although asymmetric heating alters the locations of heat generation and the pattern of fluid motion, the total heat transferred to the two sidewalls remains roughly equivalent. This study not only helps to bridge the existing knowledge gaps regarding flow transitions in multi-source plume systems, but also provides theoretical support for the utilization, suppression of flow transitions, and thermal management in engineering applications. Additionally, this research can be further extended to explore the effects of additional parameters, such as heater length ratio and heater spacing, on flow regime transitions and heat transfer performance, and can also be expanded to 3D configurations or fluids of varying Prandtl numbers (e.g., water, oil) to enhance the generalizability of the findings.

References

[1] INCROPERA F P. Convection heat transfer in electronic equipment cooling[J]. Heat Transfer,1988, 110(4): 1097-1111.

[2] YAO X, MARSHALL A W. Quantitative salt-water modeling of fire-induced flows for convective heat transfer model development[J]. Heat Transfer, 2007, 129(10): 1373-1383.

[3] HE Z, CAO Z, CHENG X, et al. Efficient inverse analysis for solving a coupled conduction, convection and radiation problem involving non-gray participating media[J]. Transactions of Nanjing University of Aeronautics and Astronautics, 2024, 41(5): 622-631.

[4] ZHANG S, FENG D, SHI L, et al. A review of phase change heat transfer in shape-stabilized phase change materials (ss-PCMs) based on porous supports for thermal energy storage[J]. Renewable and Sustainable Energy Reviews, 2021, 135: 110127.

[5] SATO T, MAEDA K, NAGATAKI S, et al. High-entropy ejecta plumes in Cassiopeia A from neutrino-driven convection[J]. Nature, 2021, 592(7855): 537-540.

[6] DESRAYAUD G, LAURIAT G. Unsteady confined buoyant plumes[J]. Journal of Fluid Mechanics, 1993, 252: 617-646.

[7] FISCALETTI D, ANGELI D, TAROZZI L, et al. Buoyancy-induced transitional flows around an enclosed horizontal cylinder: An experiment[J]. International Journal of Heat and Mass Transfer, 2013, 58(1/2): 619-631.

[8] HERNÁNDEZ R H. Natural convection in thermal plumes emerging from a single heat source[J]. International Journal of Thermal Sciences, 2015, 98: 81-89.

[9] BARRIOS G, HUELSZ G, RECHTMAN R. Heat transfer and flow transitions of a thermal plume generated by a heating element on the enclosure bottom wall[J]. European Journal of Mechanics-B/Fluids, 2019, 77: 17-24.

[10] WANG Y, SERGENT A, SAURY D, et al. Numerical study of an unsteady confined thermal plume under the influence of gas radiation[J]. International Journal of Thermal Sciences, 2020, 156: 106474.

[11] BASTIAANS R J M, RINDT C C M, NIEUWSTADT F T M, et al. Direct and large-eddy simulation of the transition of two- and three-dimensional plane plumes in a confined enclosure[J]. International Journal of Heat and Mass Transfer, 2000, 43(13): 2375-2393.

[12] GEORGE N, OOI A, MOINUDDIN K, et al. Direct numerical simulation of a turbulent line plume in a confined region[C]//Proceedings of the 20th Australasian Fluid Mechanics Conference. Perth, Australia: Australasian Fluid Mechanics Society (AFMS), 2016.

[13] GEORGE N, OOI A, PHILIP J. Evolution of a wall-attached buoyant plume in confined boxes: Direct numerical simulations, entrainment coefficient and an integral model[J]. International Journal of Heat and Fluid Flow, 2021, 90: 108824.

[14] BAINES W D, TURNER J S. Turbulent buoyant convection from a source in a confined region[J]. Jour-

nal of Fluid Mechanics, 1969, 37(1): 51-80.

[15] CHAI X, LI W, CHEN B, et al. Numerical simulation of turbulent natural convection in an enclosure with a curved surface heated from below[J]. Progress in Nuclear Energy, 2020, 126: 103392.

[16] MUKHOPADHYAY A. Analysis of entropy generation due to natural convection in square enclosures with multiple discrete heat sources[J]. International Communications in Heat and Mass Transfer, 2010, 37(7): 867-872.

[17] DURRANI F, COOK M J, MCGUIRK J J, et al. Large eddy simulation of buoyancy-driven natural ventilation-twin-plume flow[J]. International Journal of Ventilation, 2013, 11(4): 353-366.

[18] GEBHART B, SHAUKATULLAH H, PERA L. The interaction of unequal laminar plane plumes[J]. International Journal of Heat and Mass Transfer, 1976, 19(7): 751-756.

[19] ICHIMIYA K, SAIKI H. Behavior of thermal plumes from two-heat sources in an enclosure[J]. International Journal of Heat and Mass Transfer, 2005, 48(16): 3461-3468.

[20] BANERJEE S, MUKHOPADHYAY A, SEN S, et al. Natural convection in a bi-heater configuration of passive electronic cooling[J]. International Journal of Thermal Sciences, 2008, 47(11): 1516-1527.

[21] BISWAS N, MAHAPATRA P S, MANNA N K. Buoyancy-driven fluid and energy flow in protruded heater enclosure[J]. Meccanica, 2016, 51(9): 2159-2184.

[22] CENEDESE C, LINDEN P F. Entrainment in two coalescing axisymmetric turbulent plumes[J]. Journal of Fluid Mechanics, 2014, 752: R2.

[23] MEI S J, YUAN C. Three-dimensional simulation of building thermal plumes merging in calm conditions: Turbulence model evaluation and turbulence structure analysis[J]. Building and Environment, 2021, 203: 108097.

[24] LI S, FLYNN M R. Coaxial plumes: Theory and experiment[J]. International Journal of Heat and Mass Transfer, 2021, 174: 121311.

[25] GAO X, LI A, YANG C. Study on thermal stratification of an enclosure containing two interacting turbulent buoyant plumes of equal strength[J]. Building and Environment, 2018, 141: 236-246.

[26] YANG C, LI A, GAO X. Interaction of the thermal plumes generated from two heat sources of equal strength in a naturally ventilated space[J]. Journal of Wind Engineering and Industrial Aerodynamics, 2020, 198: 104085.

[27] YIN S, LI Y, SANDBERG M, et al. The effect of building spacing on near-field temporal evolution of triple building plumes[J]. Building and Environment, 2017, 122: 35-49.

[28] YIN S, SANDBERG M, LAM K, et al. Near-field merging and penetration of triple starting plumes from volumetric heat sources in a calm environment[J]. International Journal of Heat and Mass Transfer, 2017, 115: 1321-1333.

Acknowledgement This work was supported by the Tianjin Education Commission Research Program Project (No. 2024KJ105).

Author

The first/corresponding author Dr. **WANG Ying** received the M.S. degree in mechanical and aerospace engineering from École Nationale Supérieure de Mécanique et d'Aérotechnique (ENSMA), Poitiers, France, in 2016 and her Ph.D. degree in thermal engineering from La Rochelle University, La Rochelle, France, in 2020, respectively. She joined Civil Aviation University of China in April 2020, where she has been serving as a lecturer at the Sino-European Institute of Aviation Engineering. Her research focuses on natural convection, thermal radiation, and coupled heat transfer.

Author contributions Dr. **WANG Ying** designed the study, complied the models, conducted the analysis, interpreted the results, and wrote the manuscript. Prof. **YANG Wen** contributed to the discussion section and the revision of the manuscript. Mr. **XU Zhejian** contributed to the investigation process, specifically by performing the simulations and curating the data for the study. Mr. **MA Xinyu** contributed to writing the original draft of the study. All authors commented on the manuscript draft and approved the submission.

Competing interests The authors declare no competing interests.

(Production Editor: XU Chengting)

封闭腔体内双加热元件热羽流的传热特性与流动转变

王 莹，许哲健，杨 文，马鑫宇

（中国民航大学中欧航空工程师学院，天津 300300，中国）

摘要：封闭空间内多热源驱动的浮力诱导流动与传热机制是电子设备热管理、能源系统热设计等领域的核心科学问题，其精准表征对提升工程系统热效率具有关键意义。本文以底部嵌入双加热元件的二维方形封闭腔体为研究对象，以空气为工质，在（$0<Ra\leqslant1.5\times10^8$）的宽瑞利数范围内，数值模拟了总热输入恒定条件下双加热器等热通量（$q_r=1$）与不等热通量（$q_r=2$）两种工况的浮力诱导流动。通过傅里叶功率谱、相空间轨迹、最大李雅普诺夫指数等方法分析流场的流动转变特征，同时定量研究了不同工况下腔体的传热特性，包括加热器时均最高温度、等温壁面时均努塞尔数的变化规律。研究表明，两种工况下均存在系列流动转变现象，可界定为稳态、周期非稳态与混沌非稳态3类流动状态。周期流动又分为基频及其整数倍频率主导的简单周期流动，包含基频、整数倍频率及亚谐波的复杂周期流动。等热通量工况下，$Ra\leqslant2.9\times10^7$为稳态，$3\times10^7\leqslant Ra\leqslant1.3\times10^8$为简单周期流动，$1.4\times10^8\leqslant Ra\leqslant1.5\times10^8$为复杂周期流动；不等热通量工况下，稳态向周期流动的转变延迟至$5.8\times10^7\sim6.3\times10^8$，且$Ra\geqslant1.1\times10^8$时流场进入向弱混沌转变的非周期状态。等热通量工况下，加热器的时均无量纲最高温度$Ra\cdot\theta_{max}$的增长幅度介于不等热通量工况下强/弱加热器最高温度之间，且最高温度大小约为不等热通量工况下强/弱加热器的平均值。即使两加热器热通量相差一倍，腔体左右等温壁面的时均努塞尔数仍分别维持在0.46和0.54左右，散热效率基本相当。本文研究最终揭示了瑞利数、加热器热通量比对双热源热羽流浮力驱动对流系统流动转变与传热特性的关键调控机制，证实了非对称热输入会压缩周期流动的瑞利数范围、改变加热器温度响应特性，而等温壁面的散热主要由系统总热输入和对流能力决定。该研究完善了多热源羽流系统流动转变的理论体系，为电子设备被动冷却、能源系统热设计等工程场景的热管理与流动调控提供了重要的理论支撑。

关键词：自然对流；热羽流；双加热元件；流动转变；传热效率

研究亮点：

1. 在$0<Ra\leqslant1.5\times10^8$宽瑞利数范围内，系统阐明了总热输入恒定下，双加热器等热通量与不等热通量工况的热羽流流动转变规律，明确界定了稳态、周期非稳态、混沌非稳态3类流动状态及两类周期流动模式的瑞利数区间。

2. 定量揭示加热器热通量非对称分布对流动稳定性的调控机制，证实不等热通量工况会显著延迟稳态向周期流动的转变进程，且大幅压缩周期流动的有效瑞利数范围。

3. 发现双热源非对称热输入条件下，即便两加热器热通量相差一倍，腔体左右等温壁面的散热效率仍基本保持一致，不受热通量比的显著影响。

4. 建立双加热器热羽流流动基频、加热器时均最高温度与瑞利数的幂律关联模型，为多热源羽流流场的频率特征及最高温度预测提供了定量依据。